AD-A158 698 INVESTIGATION OF HIGH EFFICIENCY GENERALIZED MATCHED FILTERS(U) AERODYNE RESEARCH INC BILLERICA MA E S GAYNOR ET AL. AUG 85 ARI-RR-468 RADC-TR-85-134 1/1

UNCLASSIFIED F19628-84-C-0047 F/G 9/5 NL

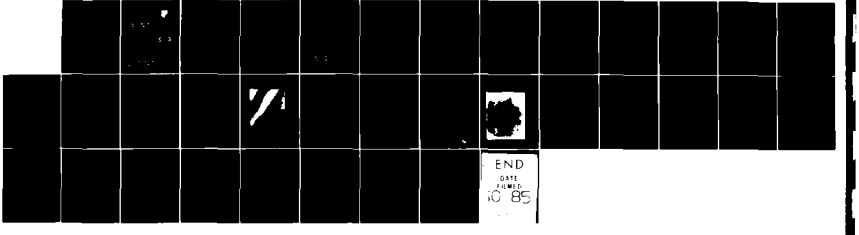

END
DATE FILMED
10 85

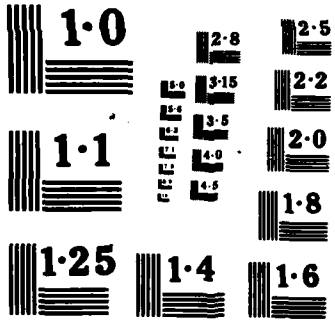
1·0
1·1
1·25
1·4
1·6
1·8
2·0
2·2
2·5
2·8
3·15
3·5
4·0
4·5
5·0

(2)

RADC-TR-85-134
Final Technical Report
August 1985

INVESTIGATION OF HIGH EFFICIENCY GENERALIZED MATCHED FILTERS

Aerodyne Research Incorporated

E. S. Gaynor
H. J. Caulfield

APPROVED FOR PUBLIC RELEASE; DISTRIBUTION UNLIMITED

ROME AIR DEVELOPMENT CENTER
Air Force Systems Command
Griffiss Air Force Base, NY 13441-5700

This report has been reviewed by the RADC Public Affairs Office (PA) and is releasable to the National Technical Information Service (NTIS). At NTIS it will be releasable to the general public, including foreign nations.

RADC-TR-85-134 has been reviewed and is approved for publication.

APPROVED: Joseph L. Horner

JOSEPH L. HORNER
Project Engineer

APPROVED: Harold Roth

HAROLD ROTH, Director
Solid State Sciences Division

FOR THE COMMANDER: John A. Ritz

JOHN A. RITZ
Acting Chief, Plans Office

If your address has changed or if you wish to be removed from the RADC mailing list, or if the addressee is no longer employed by your organization, please notify RADC (ESO) Hanscom AFB MA 01731. This will assist us in maintaining a current mailing list.

Do not return copies of this report unless contractual obligations or notices on a specific document requires that it be returned.

UNCLASSIFIED
SECURITY CLASSIFICATION OF THIS PAGE

AD-A158 698

REPORT DOCUMENTATION PAGE

1a. REPORT SECURITY CLASSIFICATION: UNCLASSIFIED	1b. RESTRICTIVE MARKINGS: N/A
2a. SECURITY CLASSIFICATION AUTHORITY: N/A	3. DISTRIBUTION/AVAILABILITY OF REPORT: Approved for public release; distribution unlimited.
2b. DECLASSIFICATION/DOWNGRADING SCHEDULE: N/A	
4. PERFORMING ORGANIZATION REPORT NUMBER(S): ARI-RR-468	5. MONITORING ORGANIZATION REPORT NUMBER(S): RADC-TR-85-134
6a. NAME OF PERFORMING ORGANIZATION: Aerodyne Research Inc. / 6b. OFFICE SYMBOL (If applicable):	7a. NAME OF MONITORING ORGANIZATION: Rome Air Development Center (ESO)
6c. ADDRESS (City, State and ZIP Code): 45 Manning Road, The Research Center at Manning Park, Billerica MA 01821	7b. ADDRESS (City, State and ZIP Code): Hanscom AFB MA 01731
8a. NAME OF FUNDING/SPONSORING ORGANIZATION: Rome Air Development Center / 8b. OFFICE SYMBOL (If applicable): ESO	9. PROCUREMENT INSTRUMENT IDENTIFICATION NUMBER: F19628-84-C-0047
8c. ADDRESS (City, State and ZIP Code): Hanscom AFB MA 01731	10. SOURCE OF FUNDING NOS.

PROGRAM ELEMENT NO.	PROJECT NO.	TASK NO.	WORK UNIT NO.
62702F	4600	19	52

11. TITLE (Include Security Classification): INVESTIGATION OF HIGH EFFICIENCY GENERALIZED MATCHED FILTERS

12. PERSONAL AUTHOR(S): E. S. Gaynor, H. J. Caulfield

13a. TYPE OF REPORT	13b. TIME COVERED	14. DATE OF REPORT (Yr., Mo., Day)	15. PAGE COUNT
Final	FROM Dec 83 TO Mar 85	August 1985	42

16. SUPPLEMENTARY NOTATION: None

17. COSATI CODES			18. SUBJECT TERMS (Continue on reverse if necessary and identify by block number)
FIELD	GROUP	SUB. GR.	Correlation, Spatial Filtering, Pattern Recognition, Phase-Only Filters
12	01		
17	07 & 08		

19. ABSTRACT (Continue on reverse if necessary and identify by block number)

In a previous RADC contract Aerodyne worked on developing an improved algorithm for reducing the rotational dependency of matched filters for use in optical pattern recognition systems. This present contract takes the final result of that effort, the so-called Generalized Matched Filter (GMF), applies the phase-only filter principle to it, and studies the results. Standard actual noisy IR images are used so the results can be compared to other such studies. Also included in this report is a brief discussion of complexity theory and how it might apply to optical computing efforts in the U.S. and elsewhere.

20. DISTRIBUTION/AVAILABILITY OF ABSTRACT	21. ABSTRACT SECURITY CLASSIFICATION
UNCLASSIFIED/UNLIMITED ☒ SAME AS RPT. ☐ DTIC USERS ☐	UNCLASSIFIED

22a. NAME OF RESPONSIBLE INDIVIDUAL	22b. TELEPHONE NUMBER (Include Area Code)	22c. OFFICE SYMBOL
JOSEPH L. HORNER	(617) 861-3841	RADC (ESOP)

DD FORM 1473, 83 APR — EDITION OF 1 JAN 73 IS OBSOLETE.

UNCLASSIFIED
SECURITY CLASSIFICATION OF THIS PAGE

EXECUTIVE SUMMARY

The joint variation of effectiveness and diffraction efficiency in computer designed pattern recognition filters was studied. Conclusions of this study include:

- The recognition of the need to eliminate spurious detail from real images before using those images to form recognition masks,
- The demonstration that fine (10°) angular sampling is not strictly necessary (20° sampling allowed recognition of intermediate angles but, of course, with diminished certainty),
- The demonstration that all available data can be included in a generalized matched filter. (The more images included the better the response to intermediate or test cases but the lesser the response to the training images. Since response to the training images is much better than needed, the tradeoff is favorable), and
- Devising a new approach to design of phase only GMF's which puts increased emphasis on phase (as opposed to amplitude) information.

Also included in this report is a brief discussion of complexity theory and how it might apply to optical computing efforts in the U.S. and elsewhere.

TABLE OF CONTENTS

INTRODUCTION

In December 1983 Aerodyne Research, Inc. (ARI) began work towards improving an improved algorithm for modeling rotation tolerant spatial frequency filters proposed for use in optical pattern recognition devices. This work was to be supported by RADC/ES for 18 months at a level of about $150 K. The contract was amended by MIPR in ~December 1984. The new contract required additional research in the area of complexity theory and the additional funding was ~$30 K. The deliverable is this Final Report of Progress.

1. INTRODUCTION TO PATTERN RECOGNITION PRINCIPLES

The art and science of optical matched spatial filtering has evolved considerably since its introduction by VanderLugt.[1] Drawbacks of matched filtering such as intolerance to scale changes and rotation of the class to be matched with respect to the matched filter (MF) have been addressed in many articles. Here the tradeoffs of within-class insensitivity vs. between-class sensitivity are well illustrated. Caulfield et al[2] surveyed progress in MF improvements. * The most recent contributions to the field of optical pattern recognition have been in appropriate definition of diffraction efficiency (DE) and suggesting methods for its improvement. Horner was the first to define a meaningful measure of the MF DE.[3] A study of filter discrimination vs. filter DE seems called for.

1.1 Fundamentals

A brief encapsulation of the concept of space invariant matched filtering for pattern recognition follows:

The amplitude distribution in the correlation plane is described as

$$\psi(x'',y'') = \iint f(x',y')\, g^{*}(x'-x'',\, y'-y'')\, dx'\, dy' \qquad (1)$$

which is the correlation of an input spatial function, f(x,y) with a reference function g(x,y). That is, g(x,y) is the pattern to be recognized. The

*Strictly speaking, a matched filter is a very particular thing which cannot be "improved" because anything else is not a matched filter. Unfortunately popular usage, to which we hereby capitulate, is to call all pattern recognition filters matched filters. The inaccuracy of this usage is compensated for by convenience.

correlation can be accomplished with a multiplication of F(x', y') and G*(x',y'), where

$$F(x'y') = \mathcal{F}[f(x,y)] = \iint f(x,y)\, e^{(-ik/\ell)(xx' + yy')}\, dx\, dy \quad , \quad (2)$$

and likewise for G(x',y'). A superscript * indicates complex conjugate, i.e.,

$$G^*(x',y') = \iint g^*(x,y)\, e^{(ik/\ell)(xx' + yy')}\, dx\, dy \quad . \quad (3)$$

Equation (1) can also be expressed as

$$\psi(x",y") = f(x,y) * g(x,y) \quad (4)$$

where * indicates correlation.

$\mathcal{F}[.]$ is the Fourier transform operator. k is $2\pi/\lambda$, the optical wave vector of wavelength λ. The coordinates [x,y] and [x',y'] are specified in the front and back focal planes of the lens of focal length ℓ used to form the transform.

In optical matched filtering systems, G*(x'y') is recorded holographically after VanderLugt.[1] The filtering operation [Eq. (1)] can be regarded as detection in the focal plane of the reconstruction of the reference plane wave used to create the holographic filter. Therefore, what is observed is

$$I(x",y") = \psi(x",y")\, \psi^*(x",y") = \left| f(x,y) * g(x,y) \right|^2 \quad . \quad (5)$$

Most improvements on VanderLugt's filter are attempts at improving their discrimination capabilities by increasing the signal-to-noise ratio in the [x",y"] plane. One of these is phase only matched filtering, reported by Horner and Gianino.[4]

2. GENERALIZED MATCHED FILTER METHOD

The intent in creating a generalized matched filter[2-3] is to maximize within class tolerance of a pattern recognition system for recognizing any given pattern to the exclusion of any others. Therefore, besides its excellent discrimination properties, the GMF is characterized by its generic nature, that is, choice of classes to be separated is arbitrary. In this case, the MF is much less versatile than the GMF and is, in fact a GMF special case. We realize the GMF with a set of computer images of variations of a spatial reference function $g_i(x,y)$ by expressing each of its points as a discriminator derived from the mean and variance from the mean of the respective point in each of a chosen subset of $g_i(x,y)$.

We start by computing the Fast Fourier Transform (FFT) at each point in each $g_i(x,y)$. The sets $\{\bar{G}_i(x'y')\}$ is the resulting collection from our i given variations of $g_i(x,y)$ data. $\bar{G}_i(x',y')$ is an MN component vector representing the FFT of the i^{th} $g(x,y)$ MxN matrix.

Now we choose appropriate samples to be representative of S in the GMF. In our case, we were given eleven computer images representing each of 11 angles to a stationary viewer of real infrared tank data. We chose six of these images.

The means and variances of each of $\bar{G}_i$ are computed point by point, collected and then reformatted into a matrix which we will call S_{MV} (means and variances). Now a statistical discriminator function is applied to each row of S_{MV}. In our case S_{MV} is a 256 x 256 real matrix and a 256 x 256 imaginary matrix consistent with our complex S $\{\bar{G}_i(x',y')\}$ tank picture FFT vector set.

This discriminator separates S_{MV} into two sets which are collections of colored noise and tank data points. $S_{MV} = S_{CN} + S_T$. Now that the set S_{MV} is optimally separated, we can express it as

$$S_{MV} = \bar{C}\,(x',y') \cdot G\,(x',y') \quad , \tag{6}$$

with $\bar{C}\,(x',y')$ the vector format of the GMF matrix.

In traditional statistical pattern recognition terms, $\bar{C}\,(x'y')$ is considered the vector which will maximize the ratio of the between to within class scatter matrices. The equation

$$[B - \lambda W]\,\bar{C} = 0 \tag{7}$$

yields λ, the maximum eigenvalue of the eigenvector $\bar{\lambda}$ which defines $\bar{C}$, the elements of the GMF. B and W are the Between and Within class scatter matrices, respectively. The classes, of course, are tanks and noise. Caulfield and Weinberg describe the elements of B and W in Ref. 3.

3. PATTERN RECOGNITION FILTER EFFICIENCY

Researchers have shown[4,5,8] that removal of amplitude yields "improved" discrimination in matched filters. In fact, much attention has been paid recently to improving pattern recognition system efficiency by means similar to the removal of amplitude in the pattern recognition filter. For instance, Lohmann and Thum[6] suggest introduction of a periodic phase mask immediately behind the input object making the Fourier spectrum of the masked object more constant in amplitude than the Fourier spectrum of the object itself. Lohmann and Thum show that a constant amplitude photographic filter made with an object and mask yields high autocorrelation intensity. This insight supports our choice of the constant maximum amplitude phase only filter for increased pattern recognition efficiency.

Bartelt[7] adds further support for phase-only matched filtering methods by suggesting that the object amplitude can be represented in the Fourier filter plane with proper choice of a phase-only kinoform K(x'y') in the input. Efficiencies approaching unity can then be achieved with introduction of another phase only kinoform $K_2(x'y')$ as a filter. This combination of a lens sandwiched between kinoforms is called a tandem component (TC) and can yield a variety of outputs depending upon the point spread function derived from the TC's combination with particular external configurations. For instance, for Bartelt's configuration of a phase mask (in effect Lohmann's system with a phase only matched filter), the point spread function in one dimension is:

$$h(x'' - x'; x') = K_1(x') \cdot K_2(x'' - x') \quad , \tag{8}$$

while the point spread function for the GMF is the familiar

$$h(x'' - x'; x') = [\delta(x'' - x)] \quad . \tag{9}$$

The impulse response (point spread function) of Eq. (9) transforms x' to a point x" dependent upon its difference from x' (space invariant) whereas the impulse response of Eq. (8) explicitly transforms x' to x" (space variant). Space variance is a property of all TC configurations. The GMF accomplishes space invariant pattern recognition filtering.

4. GMF EFFICIENCY

We will use Horner's measure to characterize GMF efficiency

$$\eta_H = \eta_M \frac{\iint \left| f(x,y) * g(x,y) \right|^2 dx\, dy}{\iint \left| f(x,y) \right|^2 dx\, dy} \tag{10}$$

where η_M is the maximum diffraction efficiency of the medium. The GMF, $C(x',y')$, is created in the Fourier plane and possesses efficiency

$$\eta_H = \eta_M \frac{\iint \left| F(x'y')\ C^*(x',y') \right|^2 dx\, dy}{\iint \left| f(x,y) \right|^2 dx\, dy} \quad . \tag{11}$$

It is apparent that the transmittance of $C^*(x',y')$ is the efficiency determining measure. Furthermore, for $\eta_M = 1$, a conceivable value, η_H will equal 1 if all amplitude information in $C(x',y')$ is removed. This is, in fact, the phase only filter where each

$$C(x'y') = A_{jk}\, e^{-i\phi_{jk}} \tag{12}$$

is divided by its respective amplitude, A_{jk} and possesses unity efficiency. ϕ_{jk} is the phase term of the x_j, y_k GMF component.

In practice, such as in our experimental data analysis, η_H will not reach unity since the integration in its numerator must be restricted to coordinates of or immediately surrounding the correlation peak.

5. EXPERIMENTS

According to the contract objective, design of experiments was meant to yield data describing the merits of the GMF and the phase-only GMF. All results were obtained using Aerodyne Research, Inc. (ARI's) PRIME 600. Programs for carrying out all data manipulations are available. Our experimental process consisted of the following five steps:

1. Preliminary tests with rotated squares,
2. Background removal and centering of supplied tank images,
3. Reduction of tank images to pure shape and GMF creation,
4. GMF tailoring and collecting data thereof, and
5. Data analysis.

5.1 Preliminary Tests

5.1.1 Generating the Rotated Squares

Computer rotation of squares proved far more difficult and perplexing than we had anticipated. We used Aerodyne's rotation algorithm in which each individual object point is rotated and the value of what point is shared among the four bounding points on the final grid as shown below:

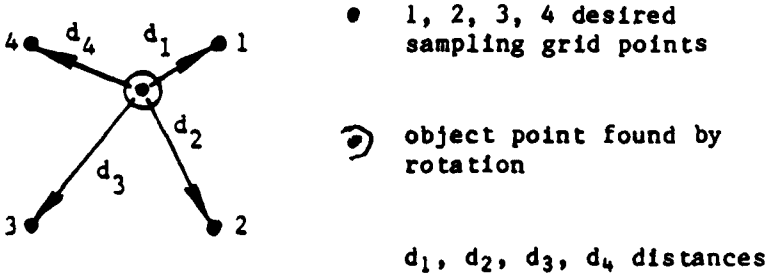

Figure 1.

If the point has a value S, we assign a value

$$S_i = (S/d_i^2)/n \tag{13}$$

where

$$n = \frac{1}{d_1^2} + \frac{1}{d_2^2} + \frac{1}{d_3^2} + \frac{1}{d_4^2} \quad . \tag{14}$$

There is no magic to the d^2. We could have used d to any other power. Note that

$$S_1 + S_2 + S_3 + S_4 = S \tag{15}$$

and that a uniform image is kept uniform by such an operation. The edges, however, present a problem. Figure 2 shows a -10° rotated square. This is a black and white copy of a pseudo colored display. It shows, as expected, that the edges of a rotated square are not sharp. When we recognize such a rotated square, what are we really recognizing: the inherent structure of rotated squares or the accidental structure introduced by our (or any other) rotation *algorithm*? *We note in Figure 2 that* the edge structure looks highly regular. Accordingly, we suspect it would be easy to recognize. If we construct a GMF from 11 rotated squares, complex conjugate it, and inverse Fourier transform it we arrive at the figure (real not nonnegative like the square) to which the GMF is matched. Figure 3 plots the amplitude of this "pseudo square." It is easy to see that

- Only high spatial frequencies (edges) count,
- The corners are especially "interesting" to the GMF, and
- Something having absolutely nothing to do with rotated squares is being recognized.

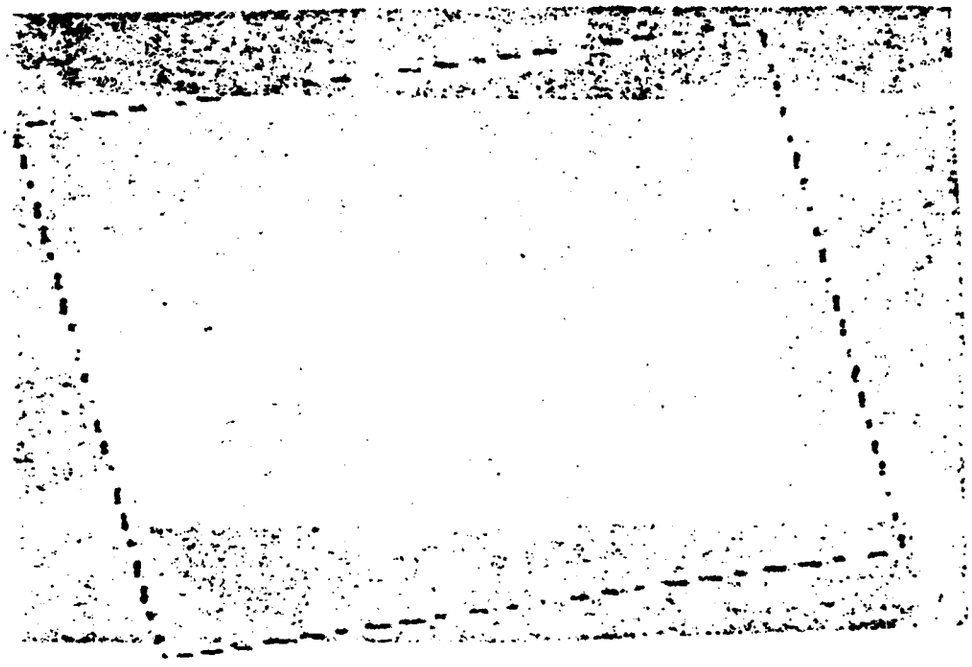

Figure 2. Unprocessed 10^{o} Rotated Rectangle

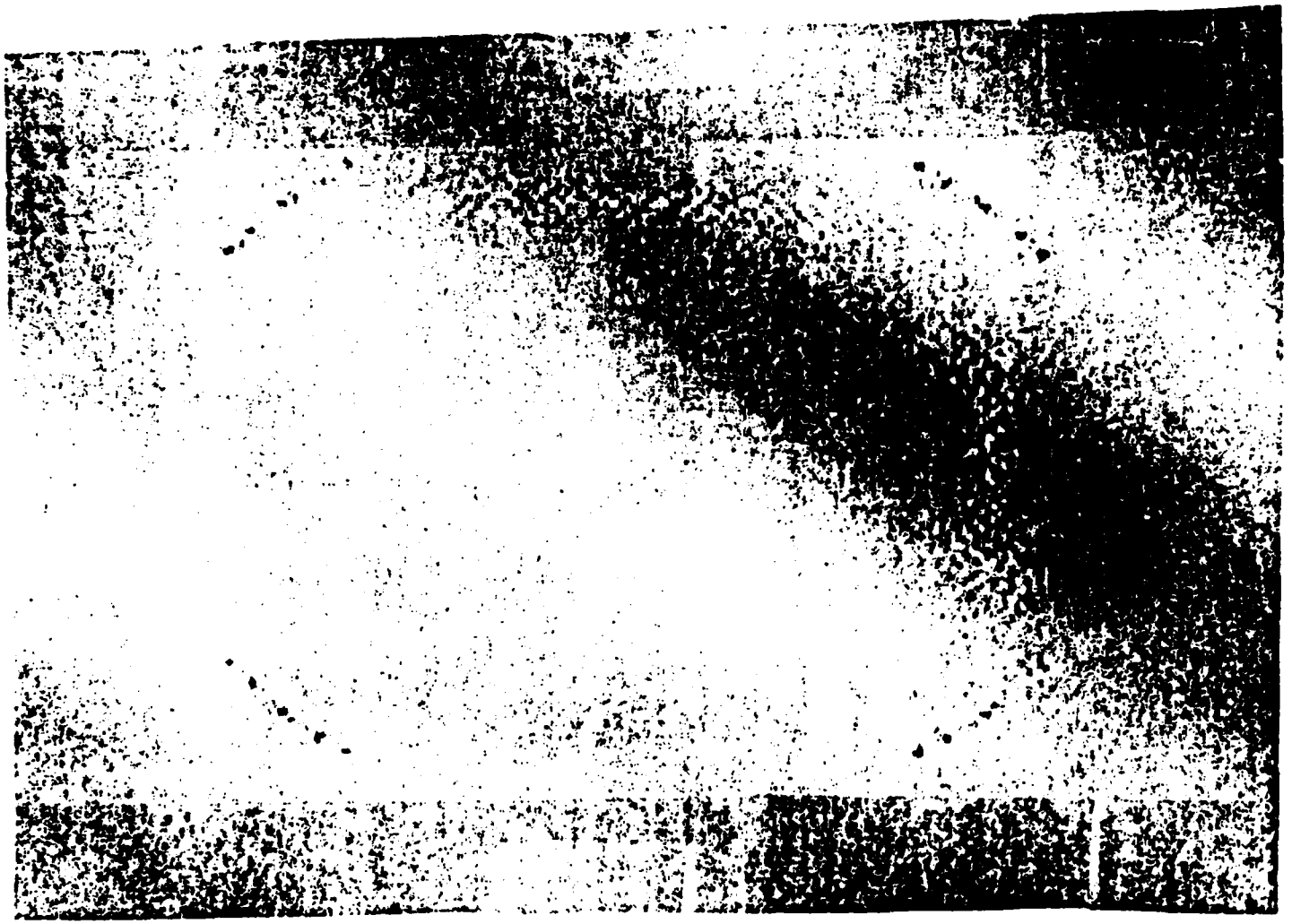

Figure 3. FFT^{-1} (GMF) of Six Rectangles

Clearly this "something extra" is the artifact mentioned earlier.

Having demonstrated the problem, we sought solutions. Unhappily the basic problem seems quite fundamental. Rotating a sampled image and then "resampling" in the original unrotated coordinate systems leads to inevitable edge artifacts. Accordingly, we sought to "smooth out" those artifacts by convolving the rotated and resampled object with a blur function. Let the rotated and resampled object be

$$o\,(x_i,\, y_j)$$

and the blur function be

$$b\,(x_i,\, y_j) \quad .$$

Then the first-order smoothed object will be

$$o^{(1)}\,(x_i,\, y_j) = \sum_{k,\ell} b\,(x_k,\, y_\ell)\; O\,(x_i - x_k,\, y_j - y_\ell) \quad . \tag{16}$$

Denoting Fourier transforms by capitals and omitting the variables conjugate to x and y for convenience, we can see that

$$O^{(1)} = BO \quad . \tag{17}$$

To avoid polarity changes in $o(x_i, y_j)$, we must make B uniphase. One function which does this is a triangular function. In a single continuous variable a triangle function like in Figure 4

Figure 4.

has a $\mathrm{sinc}^2(\cdot)$ Fourier transform which is, of course, uniphase (positive). We used the simplest triangle for b(x), i.e.

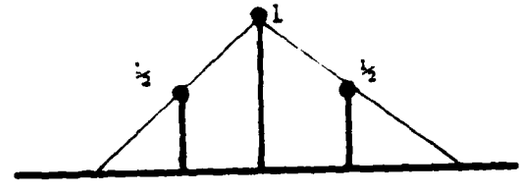

Figure 5.

In two dimensions,

$$b = \begin{vmatrix} 0 & 1/2 & 0 \\ 1/2 & 1 & 1/2 \\ 0 & 1/2 & 0 \end{vmatrix} . \qquad (18)$$

Convolving again, we have

$$o^{(2)} = o^{(1)} * b = o * (b * b) \qquad (19)$$

which represents a further blurring. Figures 6 and 7 show singly and doubly blurred -10° squares displayed as before. Some of the regularity is blurred. The "pseudo square" corresponding to a single blurring is shown in Figure 8. Clearly the "extra" information has been removed or at least greatly reduced.

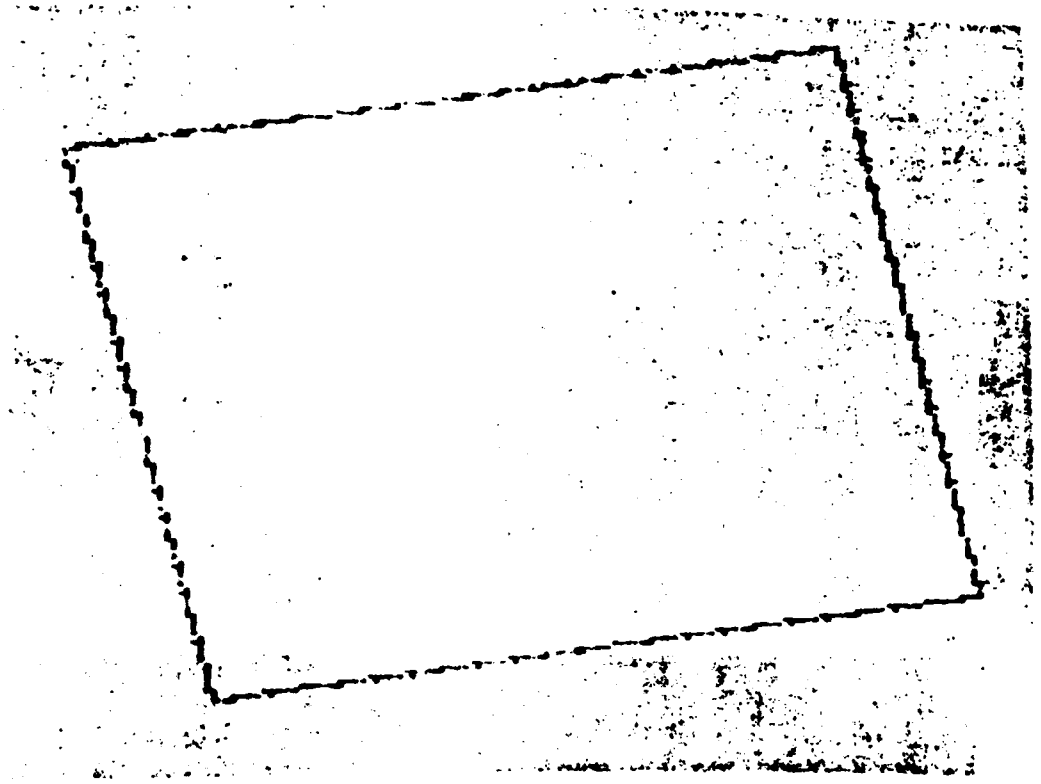

Figure 6. Once Blurred Rectangle

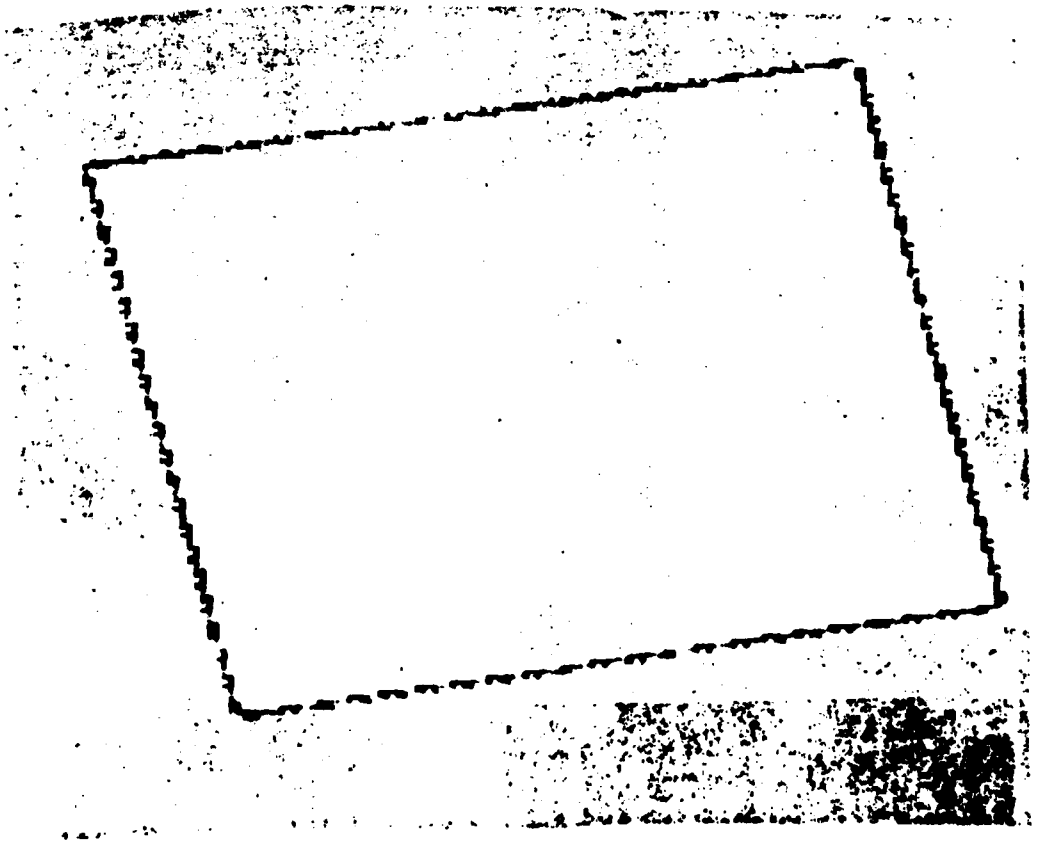

Figure 7. Twice Blurred Rectangle

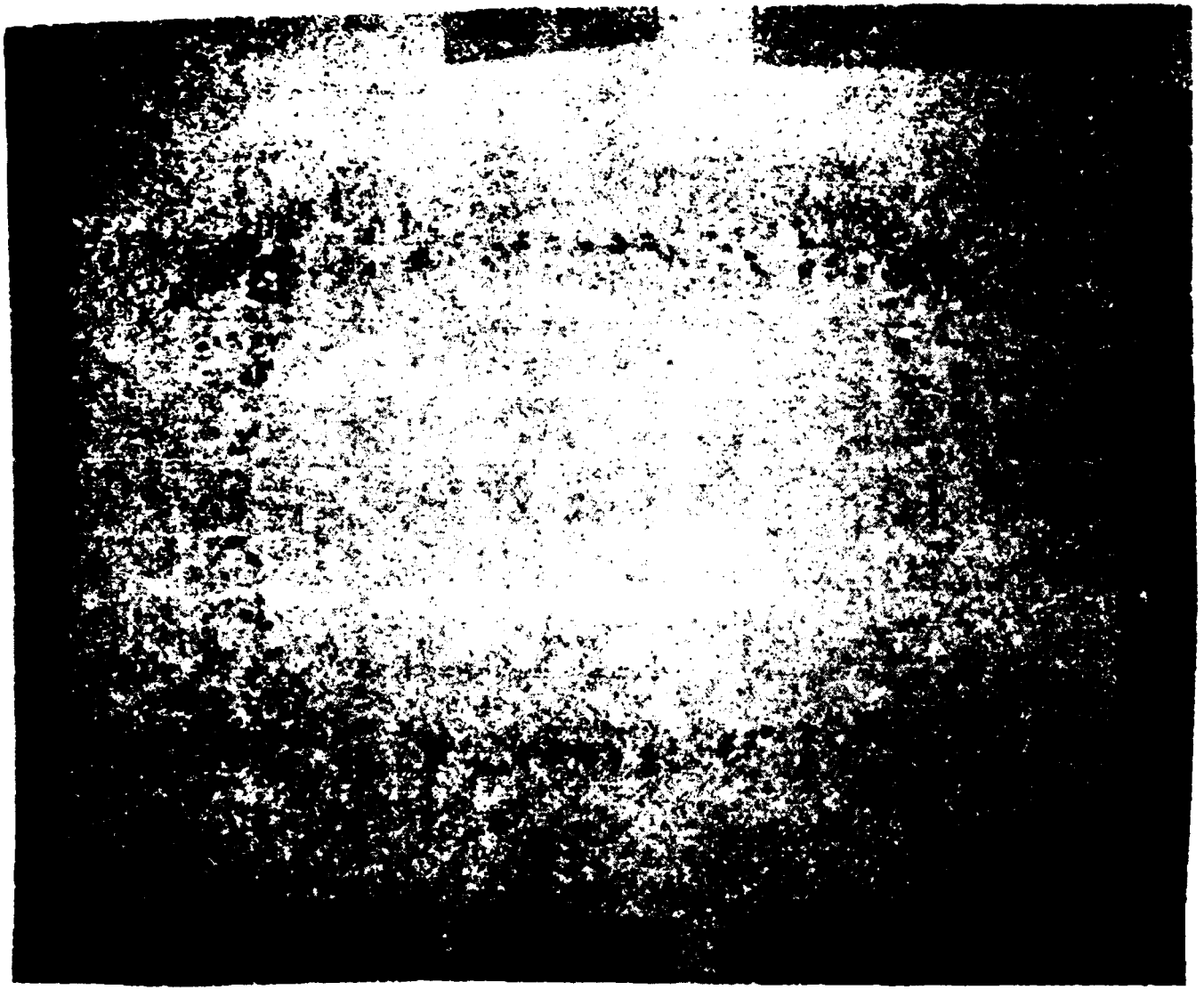

Figure 8. Final Processed FFT^{-1}(GMF) (6 Rectangles)

5.2 Background Removal and Centering

The tank imagery we received contained tank outlines with an overlay of random pixel values corresponding to noise in the background as well as in the imaging apparatus and the illumination conditions. In addition, the tank outlines were displaced from the center of their respective frames. In creating the GMF, and in using it for correlations, centered images with clear backgrounds are desirable in order that 1) Coordinates of correlation peaks can be positively identified and 2) Background random noise spectra are excluded from those of the tank. Therefore, we designed a program which allowed us to outline the tank by hand with a cursor and joystick and to place the geometric center of the resulting tank outline at the center of the frame.

5.3 Reduction of Images to Binary

What remained after the previous step were the outlines of tanks with overlays of nearly indiscernable structure mixed with random scatter representing the particular (unknown) illumination. A GMF was created using six of these eleven images. Correlations with images less background in both the six used and the five not used sets were generated. Scans of the row and column containing the greatest correlation plane amplitude were used in the analysis. In this case, we saw no correlation. Therefore, since the intent is to correlate shape, and not scattered light content within the shape, we created an improved GMF after setting all amplitudes with the images of the incorporated tanks equal to 1, retaining, as before, zero background. This GMF, upon correlation with the tanks with scattered light, both within and outside of the incorporated set yielded positive results.

The theoretical validity of this approximation was proven by Horner for one dimension in a private communication as follows:

Let input = $f(x)$

Noisy input = $f(x) + n(x)$

"Clean" filter = $h(x) = f(x-x_o)$

"Dirty" filter = $h'(x) = f(x-x_o) + n(x)$

Case 1: Correlation with "clean" filter

$$R = f(x) * h(x) = \left[f(x) + n(x)\right] * f(x-x_o) = R(x-x_o) + n(x) * f(x-x_o) \tag{20}$$

Case II: Correlation with "dirty" filter

$$R = f(x) * h'(x) = \left[f(x) + n(x)\right] * \left[f(x-x_o) + n(x)\right] \tag{21}$$

$$= R(x-x_o) + n(x) * f(x-x_o) + n(x) * f(x) + n(x) * n(x) \tag{22}$$

If n(x) is white, the third term clearly can be neglected. Otherwise the difference between Case I and Case II depends upon the degree to which f(x) looks like noise. If this degree is significant, both Case I and Case II are severely limited. Of course, the fourth term by the random nature of n(x), goes to zero. Therefore, the validity of binarizing our training set inputs is summarily proven.

5.4 GMF Tailoring

Next we proceed to progressively bias the GMF towards a record of phase only information. This is accomplished most dramatically by progressively removing edge pixels. This is because the GMF, unlike Matched Filter, transmits more light at its edges (high spatial frequency correlation) than in its center. The O, π phase structure is evenly distributed, however, and, thus, the progression toward a phase-only case can be shown.

To achieve the maximum Horner efficiency, we set the highest transmission (generally near the highest spatial frequency) to unity. Thus we vary the efficiency by 1) varying the maximum spatial frequency and 2) renormalizing for each spatial frequency. Naturally, lower maximum spatial frequencies have higher Horner efficiencies because all objects have (on the whole) more low frequency than high frequency power.

The implementation of this technique is as follows:

- o Normalize 256 x 256 GMF to its highest amplitude (transmission)
- o Observe correlation with input
- o Remove all but center 128 x 128 pixels
- o Renormalize
- o Observe correlation
- o Remove all but center 64 x 64 pixels
- o Renormalize
- o Observe correlation
- o Remove all amplitude by dividing each one by itself
- o Observe correlation

We observed the correlations by scanning across the row and column of the maximum output signal.

This manipulation of filter spatial frequencies should yield the relationship between GMF discriminating ability and efficiency as the GMF is progressively low frequency biased.

5.4.1 Statistical Analysis

Table 1 contains three measures of a filter's merit. All data was extracted from row and column traces through the maximum value pixel in the computer simulated correlation of the GMF with each of five input angle variations, all out of the training set which formed the GMF. All of these measures will be defined below.

Table 1 - Three Figures of Merit of the GMF

Format	F	Clustering Coefficient	η_H Relative
Phase Only (256 x 256)	2.9	12	1
64 x 64	2.66	13.2	3.1×10^{-4}
128 x 128	1.56	33.8	1.2×10^{-5}
256 x 256	1.9	45.4	9.0×10^{-5}

$$\text{The Fisher Criterion, } F = \frac{\text{Av } [I_i]_{(I_i \varepsilon S_T)} - \text{Av } [I_i]_{(I_i \varepsilon S_N)}}{\frac{1}{2} \text{Av } [I_i - I_j]_{(I_i, I_j \varepsilon S_T)} + \frac{1}{2} \text{Av } [I_i - I_j]_{(I_i, I_j \varepsilon S_N)}} \tag{23}$$

represents rotation tolerance as the ratio of the determinants of the Between (B) to Within (W) class scatter matrices for:

S_T = set of all inputs corresponding the class of tanks

S_N = set of all inputs not corresponding to tanks

I_i = detected signal when the i^{th} input pattern I_i is presented.

The class S_N is represented by the second largest magnitude in any of the ten (five row, five column) traces through the five correlations. Thus, noise is biased high with an average value figured from among the largest noise responses. Subjectively, this noise spike is typical of the signal which will most likely trigger a false correlation response.

The Clustering Coefficient represents rotation tolerance of the GMF but is also an indicator of confidence level in other figures of merit. The coefficient was calculated by averaging the magnitudes of the distances of the output maxima from the center output pixel. Therefore, since in space invariant filtering systems, the correlation peak is in theory at the center of the output plane for an input on axis, the clustering coefficient represents filtering system error. It is significant that in the phase-only and 64 x 64 case the similar average clustering coefficient was calculated from even more similar correlation peak placements. Presumably, the errors are predictable and are unique to the input rotation angle. Since these errors are predictable, they are correctable, and additional manipulation of the data has lead to this improvement.

The Horner efficiency, η_H is described in detail in a previous section. It is presented in Table 1 as the average of the largest correlation pixel intensities for non-training set inputs, normalized to the case of the phase only GMF format. Actual η_H will be quite different because each peak

correlation intensity will be normalized to the integrated input f(x,y) intensity. Normalization to the phase-only case is for demonstration of its virtue, in particular. As a matter of interest, our largest observed η_H (for inputs within the training set) is approximately one order of magnitude greater than the average over non-training set cases presented.

This data represents our progress to October 84. Since then we have drawn other conclusions based on further data. In particular, it is necessary to characterize the Generalized Matched Filter and its Phase only counterpart in terms of three system parameters: Signal-to-Noise Ratio (SNR), Efficiency (η_H), and False Alarm Figure. To obtain this data, it is of primary importance to positively identify the correlation peak. The following discussion targets this issue.

5.4.2 Clustering Coefficient

The preliminary data above consists of row and column traces in the output plane through the maximum value pixel. We based our figure of merit data on these intensity values. The clustering coefficient was also presented as a level of credibility of the other figures of merit, F, and η_H. The clustering coefficient is the average distance of the observed maximum correlation intensity for inputs out of the training set from the center pixel in the output plane for each filter format. We have found, however, that to expect the correlation maxima to occur at the center pixel is not valid. This we know since training set maxima, which are very sharply peaked occur at near center pixels. It is intuitively clear that the centering of individual elements of the composite FFT^{-1} {GMF} (impulse response) will not be perfect and, therefore, the cross correlations of this impulse response and non-training set inputs will be even less perfect.

A possible explanation for this fact is that the centering information (moments) of the training set members is calculated using the internal pixels of the tank image while the composite filter retransforms only training set member edges. These edges distinctly appear in the retransformation of the

GMF, and their centering will not in general be the same as that of the mass-centered input.

Now that we have the virtual centers, we can look there for the correlation peak and use an average clustering coefficient to define a small area around the virtual center wherein the peak should be found. If this peak is not sufficiently distinct from noise, or if greater valued peaks exist elsewhere, then the filter must be suspect. Our SNR and η_H figures will be based on the greatest valued pixel in the area of the virtual center. Peaks of greater magnitude will be tabulated as false alarms. The average clustering coefficient is about five pixels. This defines one half of a square dimension to be drawn about the virtual center and probed for a maximum.

False Alarm Figure

The false alarm figure is the number of pixel values outside of the above described area surrounding the virtual center which have equal or greater value.

Signal To Noise Ratio (SNR)

The signal is determined by the maximum pixel value in an area within five pixels (- radius) of the virtual center. The noise is the sum of all output values outside of the first minimum in the signal envelope. This envelope typically comprises a radius of three of four pixels.

Horner Efficiency

η_H is determined as the ratio of the signal defined above to the summed pixel values in the input.

5.5 Latest Data and Analysis

These data are presented in Table 2.

Table 2

		False Alarm (#)	SNR	η_H(%)
$Ae^{i\phi}$	256	115	5	1.4×10^{-5}
	128	67	4.1	1.9×10^{-3}
	64	124	4.5	1.7×10^{-4}
$e^{i\phi}$	256	57	4.2	3.4×10^{-1}
	128	208	3.4	3.9×10^{-2}
	64	325	3.4	3.9×10^{-2}

Latest data based on virtual center - derived maximum correlation signal intensities. $Ae^{i\phi}$ - amplitude and phase GMF; $e^{i\phi}$ - phase only GMF. Indicated values are averages over the three orientations of input tanks 10°, 50°, 90°.

The following remarks are to help clarify the data.

1) First, tank images of only three orientation angles outside of the training set were available for these experiments. These orientations are 10°, 50°, and 90° angle to the viewer of the longitudinal axis (along gun barrel) of the tank. Our feeling is that the 10° image carries the least and 90° the greatest amount of tank-specific information. Indeed, the data support this intuition.

2) Second, filters of various spatial extent were tested in both the phase-only and amplitude and phase cases. We would expect little deviation in the data between different size phase-only filters and marked differences between various sized amplitude and phase filters. This is because, in a GMF, amplitude transmittance is greatest at the edges whereas phase values are distributed evenly. The data presented here is by this test inconclusive except for our η_H data which are more alike for $e^{i\phi}$ than for $Ae^{i\phi}$ filters.

There is, however, a trend among all the $Ae^{i\phi}$ data which is not present in the $e^{i\phi}$ data. Performance is best across the board for smaller (64 x 64) filters, dips and then improves again to a lesser degree for large (256 x 256) filters. We observed this same trend in our pre-October data (Table 1).

What is apparent from the data in Table 2 is that the efficiency of phase-only filters is superior. It is also apparent that SNR is adequate. But the shortcoming of the GMF seems to be in its false alarm figure. This is clearly gross sub-spec performance. The interesting note about the false alarm figure is that for the 90° orientation, it is much lower than average, ranging from zero to three for both $Ae^{i\phi}$ and $e^{i\phi}$. This suggests an input dependent and not algorithm-dependent problem and therefore, the GMF concept should not yet be questioned. A solution may be a weighing of training set orientations which are "hard to recognize" i.e., tanks pointed at the observer. In addition, centering training set entrants by their outlines may clear up the problem of scattered peaks, (see Figure 9) thus ensuring the right choice in the correlation plane. In general, improvement in the false alarm figure is apparently possible with some filter manipulations.

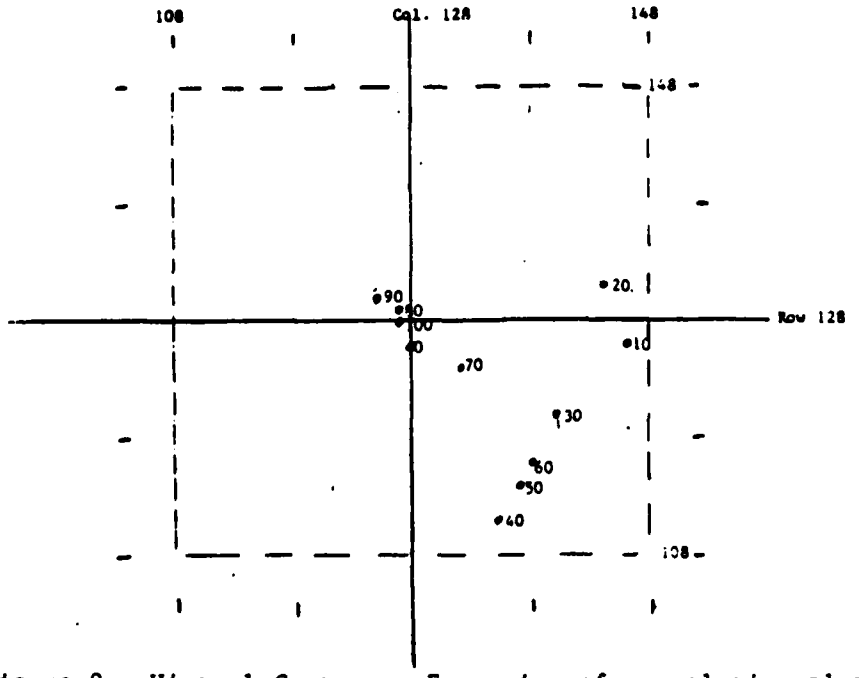

Figure 9. Virtual Centers. Expansion of correlation plane center. Dashed lines enclose center 40^2 (= 1600) pixels. Numbers represent input orientation yielding the virtual center. (DEGREES)

6. FUTURE WORK

The work performed in this contract has given us a reasonable understanding of the experimental performance of the GMF. Some advantages and disadvantages have been pointed out, and the feasibility of frequency-plane averaging for rotation tolerance has been thoroughly demonstrated. One specific algorithm improvement has been proven necessary. It is described below.

6.1 Use of Complex Numbers

The generalized matched filter (GMF) algorithm transforms the 2D array of complex expected values and variances into a 1D signal for subsequent processing to find an "optimum linear discriminant." The optimum linear discriminant (a 1D signal) is then inverse transformed to a 2D array of complex values which constitutes the GMF. Professor William T. Rhodes made an insightful remark on this process: "You are free to use any 2D to 1D transformation." Let us expand on that remark.

In deriving the GMFs for this report, we represented the complex number

$$n = x + iy = A \exp(i\emptyset) \tag{24}$$

by the two numbers x and y. This gives equal importance to the real imaginary parts. This seems sensible. Analysis by Horner[8] suggests that $\emptyset$ is much more important than A in pattern recognition. This suggests two other approaches which should lead to improved GMFs:

- Use A and $\emptyset$ rather than x and y or
- Use $\emptyset$ only.

The former gives a nonlinear emphasis on $\emptyset$. The latter gives a phase only GMF. In addition to this clear improvement in the GMF algorithm, future work should concentrate on actual production of optical Fourier-plane phase-only filters. These will probably best take the form of on-axis kinoforms encoded by computer to properly phase mask the spatial frequency content of the spatial information input to a target identification optical computer. Aerodyne Research, Inc. (ARI) has designed a method for making such phase masks using bleached photographic plates or film. Binary phase representations based on 0, π phases only can also be generated in this manner.

6.2 Phase Only GMFs

We believe that the phase-information-enhanced phase only MFs and GMFs (based on the analysis of Subsection 6.1) represent a very significant direction for future development.

7. ACKNOWLEDGEMENT

The authors would like to acknowledge the invaluable assistance of M. Weinberg of ARI with programming and taking of raw data.

8. REFERENCES

1. A. VanderLugt, IEEE Trans. Int. Theory II-10, p. 139 (1964).
2. H.J. Caulfield, R. Haimes, D. Cassesent, Opt. Eng. 19, p. 152 (1980).
3. H.J. Caulfield and M.H. Weinberg, Appl. Opt. 21, p. 1699 (1982).
4. J.L. Horner and P.D. Giannino, Appl. Opt. 23, p. 812 (1984).
5. H.J. Caulfield, Appl. Opt. 21, p. 4391 (1982).
6. A. Lohmann, C. Thum, Appl. Opt. 23, p. 1503 (1984).
7. H. Bartelt, Appl. Opt. 23, p. 1499 (1984).
8. J.L. Horner, Appl. Opt. 21, p. 4511 (1982).

MISSION
of
Rome Air Development Center

RADC plans and executes research, development, test and selected acquisition programs in support of Command, Control Communications and Intelligence (C^3I) activities. Technical and engineering support within areas of technical competence is provided to ESD Program Offices (POs) and other ESD elements. The principal technical mission areas are communications, electromagnetic guidance and control, surveillance of ground and aerospace objects, intelligence data collection and handling, information system technology, solid state sciences, electromagnetics and electronic reliability, maintainability and compatibility.

Printed by
United States Air Force
Hanscom AFB, Mass. 01731

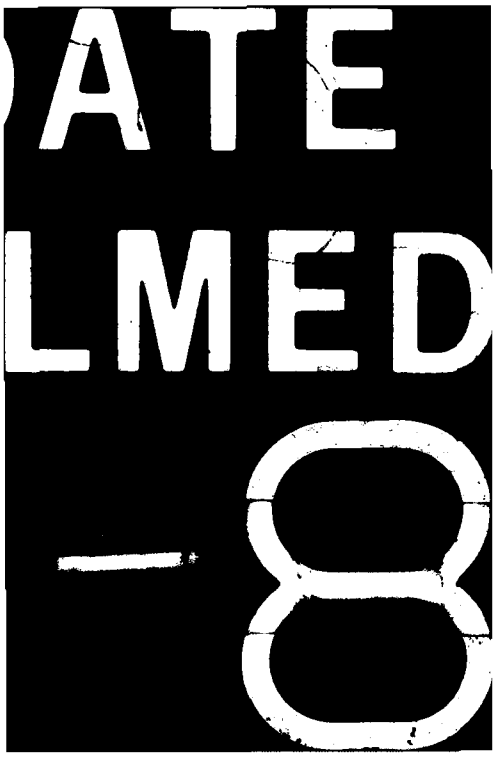
ATE
LMED
-8